Impact of Digital Control Delay on Stability of Grid-Following Converters

Gao, Xian; Zhou, Dao; Anvari-Moghaddam, Amjad; Blaabjerg, Frede

Published in:
Proceedings of the 2022 IEEE 13th International Symposium on Power Electronics for Distributed Generation Systems (PEDG)

DOI (link to publication from Publisher):
10.1109/PEDG54999.2022.9923157

Publication date:
2022

Document Version
Accepted author manuscript, peer reviewed version

Impact of Digital Control Delay on Stability of Grid-Following Converters

Xian Gao
AAU Energy
Aalborg University
Aalborg, Demark
xiga@energy.aau.dk

Dao Zhou
AAU Energy
Aalborg University
Aalborg, Demark
zda@energy.aau.dk

Amjad Anvari-Moghaddam
AAU Energy
Aalborg University
Aalborg, Demark
aam@energy.aau.dk

Frede Blaabjerg
AAU Energy
Aalborg University
Aalborg, Demark
fbl@energy.aau.dk

***Abstract*—In a digital controlled system, the delay is inevitable. It will change the phase-frequency characteristics of the system, which will affect the stability. This paper analyzes the configuration of the grid-following converter and builds its small-signal model in detail. The impacts of delay on the stability of grid-following converters are analyzed through impedance-based model and single-input single-output (SISO) transfer function. In order to achieve a fair comparison, the two stability analysis methods are applied to the same system. Finally, a time-domain simulation model of 7 kW grid-following converter is built in Matlab/Simulink and an experimental prototype with same parameters is carried out to verify the effectiveness of the theoretical analysis.**

Keywords—Digital delay, grid-following converter, stability analysis methods, impedance-based model, SISO transfer function

I. INTRODUCTION

With the depletion of traditional fossil energy, more and more distributed renewable energy is required and needs to be connected to the power grid. As an important interface between the distributed generation system and the power grid, the grid-connected inverter has attracted extensive attention.

The conventional grid-following control is widely applied in renewable energy systems and it mainly uses digital pulse width modulation (PWM) to trigger underlying switch components [1]. In such digital controlled systems, the inherent digital control delay introduced by analog to digital conversion, digital processor computation, and PWM generation is inevitable [2], [3]. Digital control delay will change the phase-frequency characteristics of the system, influence the bandwidth of control loops and the dynamic performance, and even cause the instability of the grid-connected system [4]. It is necessary to analyze the impact of digital control delay on the performance of grid-following converters.

To analyze the stability of the power system, state-space method, impedance model, and single-input single-output (SISO) transfer function are well known [5]. The eigenvalue analysis method based on the state-space model can judge the stability of the system accurately. The dynamic equations of the system are linearized at the steady-state operation point, and then the state-space model of the system can be established. The eigenvalues, eigenvectors and participation factors of the state-space matrix are solved, while stability of the system is judged by the distribution of eigenvalues on the complex plane. However, the state-space method is very complicated and needs a thorough knowledge of the system, which is normally not practical. In addition, the state-space matrix does not distinguish the relationship between state variables, so it is difficult to analyze the dynamic interaction between internal systems [6].

The impedance model is considered from the system level. Each subsystem establishes the corresponding impedance model according to its own parameters and control strategy, expresses its external characteristics in the form of impedance, and then analyzes the system stability according to the impedance ratio. In this method, the power grid and inverter are regarded as two independent subsystems respectively [7]. Because the two subsystems are independent, when the parameters in the subsystem change, the mathematical models of other subsystems are not affected, and there is no need to re-establish the system model according to the changes of parameters. Therefore, when it is applied to the system stability analysis, the difficulty of system modeling is reduced. The stability of the overall system can be judged by whether the ratio between the grid impedance and converter impedance satisfies the Nyquist stability criterion.

The SISO transfer function is commonly used to analyze the stability of the system in the classical control theory. Through the SISO open-loop transfer function, the influences of different parameters on the system stability margin can be quantitatively studied, and it is easy to analyze the dynamic interaction between each control loop. The feedback system is stable when the phase margin of the open-loop transfer function is positive, increasing the phase margin can also improve the performance of the transient response, which can serve as guidelines for systematic design and stability evaluation in a practical project. For the grid-connected converter, as the modeling is multi-input and multi-output (MIMO) when the phase-locked loop (PLL) unit is taken into account, it is not easy to get the stable operational range. In order to simplify the analysis and get the stability margins, a lot of papers worked on converting MIMO model into SISO equivalent model [8], [9].

According to the analysis above, this paper applies the impedance model based on the Nyquist plots and the SISO transfer function based on the Bode plots to analyze the stability of the grid-following converter. The rest of the paper is organized as follows. Section II illustrates the modeling of grid-following converters. In Section III, the impedance model approach based on Nyquist plots and the SISO open-loop

This work was supported by the State Scholarship Fund of China Scholarship Council (CSC).

transfer function approach based on Bode plots are applied to compare the stability analysis results. In Section IV, a time-domain simulation model is built in Matlab/Simulink to verify the theoretical stability analysis. In Section V, experimental results are presented. Finally, Section VI concludes the work.

II. Modeling of Grid-Following Converters

A. Configuration of Grid-Following Converters

The control scheme of a typical grid-following converter is shown in Fig. 1. The control scheme includes a current loop, a PLL and the PWM unit [10]. It needs to be noted that the PLL may influence the stability of the grid-connected system, but these influences can be eliminated by decreasing the bandwidth of the PLL or using some improved structure of the PLL [11]. This paper focuses on the effects of digital control delay and the impact of PLL is not the subject of this paper, so in order to simplify the analysis, the effects of the PLL and the coupling between d-axis and q-axis are not considered. U_{dc} is the dc-link voltage; L_f and C_f are the filter inductance and the filter capacitance; The grid impedance is represented as $Z_g=R_g+j\omega L_g$, where L_g and R_g are the equivalent inductance and resistance of the grid; U_{pcca}, U_{pccb} and U_{pccc} are the voltages at the point of common coupling (PCC); U_a, U_b and U_c are the converter voltages; U_{ga}, U_{gb} and U_{gc} are the grid voltages; i_a, i_b and i_c are the converter currents.

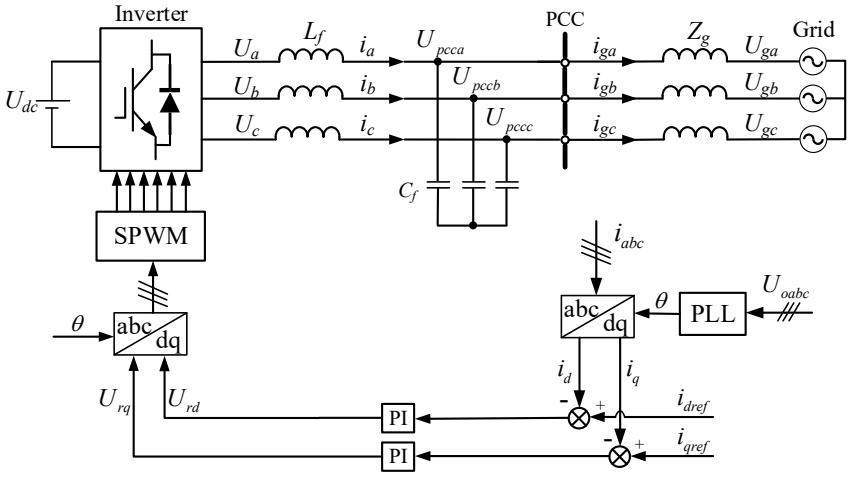

Fig. 1. Control scheme of the grid-following converter.

B. Impedance Model

According to the Kirchhoff's voltage law and the Laplace transformation, the small-signal expressions of the electrical system can be given as [12]:

$$\begin{bmatrix}\Delta U_{pccd}\\ \Delta U_{pccq}\end{bmatrix}-\begin{bmatrix}\Delta U_{gd}\\ \Delta U_{gq}\end{bmatrix}=\begin{bmatrix}sL_g+R_g & 0\\ 0 & sL_g+R_g\end{bmatrix}\cdot\begin{bmatrix}\Delta i_{gd}\\ \Delta i_{gq}\end{bmatrix}=B_{L_g}\cdot\begin{bmatrix}\Delta i_{gd}\\ \Delta i_{gq}\end{bmatrix} \quad (1)$$

$$\begin{bmatrix}\Delta i_{Cd}\\ \Delta i_{Cq}\end{bmatrix}=\begin{bmatrix}sC_f & 0\\ 0 & sC_f\end{bmatrix}\cdot\begin{bmatrix}\Delta U_{pccd}\\ \Delta U_{pccq}\end{bmatrix}=B_{C_f}\cdot\begin{bmatrix}\Delta U_{pccd}\\ \Delta U_{pccq}\end{bmatrix} \quad (2)$$

$$\begin{bmatrix}\Delta U_d\\ \Delta U_q\end{bmatrix}-\begin{bmatrix}\Delta U_{pccd}\\ \Delta U_{pccq}\end{bmatrix}=\begin{bmatrix}sL_f & 0\\ 0 & sL_f\end{bmatrix}\cdot\begin{bmatrix}\Delta i_d\\ \Delta i_q\end{bmatrix}=B_{L_f}\cdot\begin{bmatrix}\Delta i_d\\ \Delta i_q\end{bmatrix} \quad (3)$$

where subscripts d and q denote d-axis and q-axis components of a variable; Δ denotes a small-signal perturbation of a variable; s is the Laplace variable.

A single current control loop is adopted in this paper. The converter currents are regulated through a traditional PI controller. The output of current control loop is then served as the voltage reference for the PWM unit. The small-signal expressions of the current loop can be given as:

$$\begin{aligned}\begin{bmatrix}\Delta U_{rd}\\ \Delta U_{rq}\end{bmatrix}&=\begin{bmatrix}k_p+\frac{k_i}{s} & 0\\ 0 & k_p+\frac{k_i}{s}\end{bmatrix}\cdot\left(\begin{bmatrix}\Delta i_{dref}\\ \Delta i_{qref}\end{bmatrix}-\begin{bmatrix}\Delta i_d\\ \Delta i_q\end{bmatrix}\right)\\ &=\begin{bmatrix}G_i & 0\\ 0 & G_i\end{bmatrix}\cdot\left(\begin{bmatrix}\Delta i_{dref}\\ \Delta i_{qref}\end{bmatrix}-\begin{bmatrix}\Delta i_d\\ \Delta i_q\end{bmatrix}\right)=B_{PI\_i}\cdot\left(\begin{bmatrix}\Delta i_{dref}\\ \Delta i_{qref}\end{bmatrix}-\begin{bmatrix}\Delta i_d\\ \Delta i_q\end{bmatrix}\right)\end{aligned} \quad (4)$$

where k_p and k_i represent the proportional and the integral coefficients of the current control loop, respectively.

In the digital-controlled system, the delay is inevitable. When the sampling frequency is equal to the switching frequency, the delay includes one sampling period caused by the computational delay and a half sampling period caused by the PWM delay [13]. As a result, the delay unit can be modeled as:

$$B_{del}=\begin{bmatrix}e^{-1.5T_{sa}s} & 0\\ 0 & e^{-1.5T_{sa}s}\end{bmatrix}=\begin{bmatrix}e^{-T_ds} & 0\\ 0 & e^{-T_ds}\end{bmatrix}=\begin{bmatrix}G_{delay} & 0\\ 0 & G_{delay}\end{bmatrix} \quad (5)$$

where T_{sa} is the sampling period and T_d is the delay time.

Because the delay time T_d is very small, in order to simplify the model, the first-order Taylor series is often applied. The delay unit is roughly represented as an inertia unit [14]:

$$G_{delay}=e^{-T_ds}\approx\frac{1}{1+T_ds} \quad (6)$$

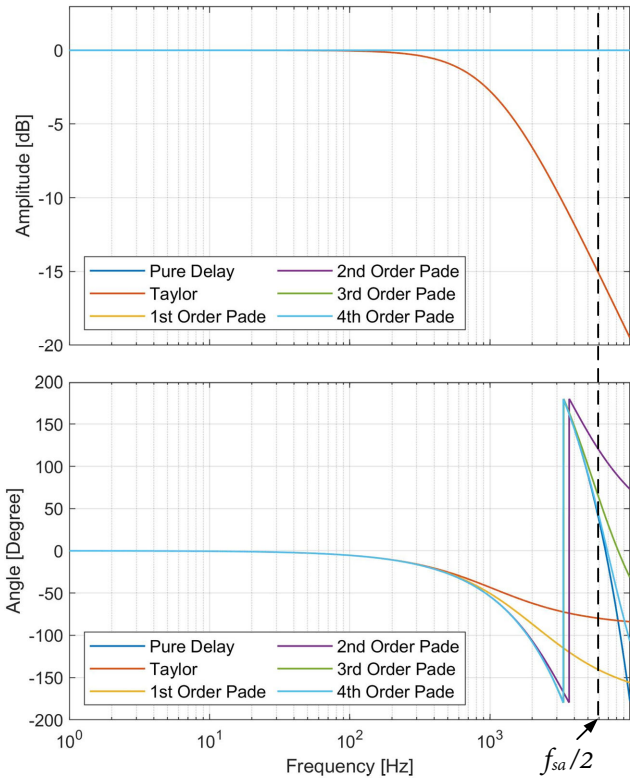

Fig. 2. Bode plots of different approximation methods to represent the delay unit.

However, the first-order Taylor series is very inaccurate at the high-frequency range. The Bode plots of first-order Taylor series and Pade approximations with different orders are shown in Fig. 2. As shown in Fig. 2, the pure delay and Pade approximations with different orders have the same amplitude-frequency characteristic. In this paper, the third-order Pade approximation is applied to reduce the complexity while making the model accurate enough within the half of the sampling frequency, which is given as [15]:

$$G_{delay} = e^{-T_d s} \approx \frac{120 - 60T_d s + 12(T_d s)^2 - (T_d s)^3}{120 + 60T_d s + 12(T_d s)^2 + (T_d s)^3} \tag{7}$$

According to Thevenin and Norton equivalent theorem [16], the grid-following converter is equivalently divided into converter and grid subsystems, which is shown in Fig. 3.

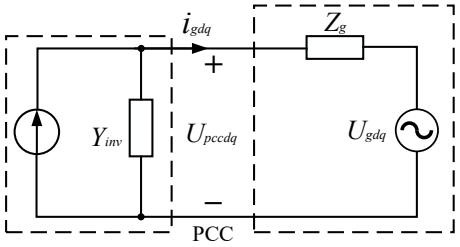

Fig. 3. Equivalent circuit of the grid-following converter.

Since two subsystems are regarded as independent, based on (1)-(5), the small-signal control structure of the grid-following converter is shown in Fig. 4. The equivalent admittance Y_{inv} and impedance Z_g can be used for stability analysis.

The impedance ratio between the grid-side impedance and the converter-side impedance can be used for Nyquist stability criterion to analyze the system stability. According to Fig. 4, the equivalent admittance of the converter and the equivalent impedance of the grid can be given as:

$$Y_{inv}(s) = \left(B_{Lf} + B_{del}B_{PI\_i}\right)^{-1} \tag{8}$$

$$Z_g(s) = \left(B_{Lg}^{-1} + B_{Cf}\right)^{-1} \tag{9}$$

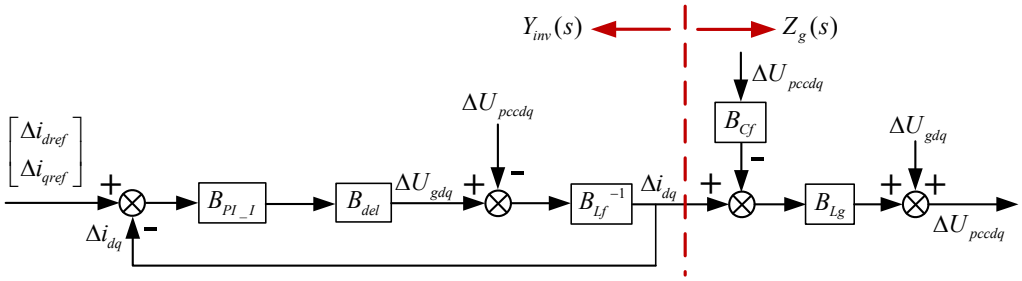

Fig. 4. Small-signal control structure of the grid-following converter.

C. SISO Transfer Function

Because the effects of the PLL and the coupling between the d-axis and q-axis are not considered, the control of the d-axis and q-axis components are the same. Hence, the analysis can be demonstrated only on the d-axis. According to the control block diagram of the grid-following converter shown in Fig. 5, the open-loop transfer function from the input i_{dqref} to the output i_{dq} can be calculated as:

$$G_{open} = \frac{G_i G_{delay}\left[sC_f(sL_g + R_g) + 1\right]}{s^3 L_g L_f C_f + s^2 R_g L_f C_f + (L_g + L_f)s + R_g} \tag{10}$$

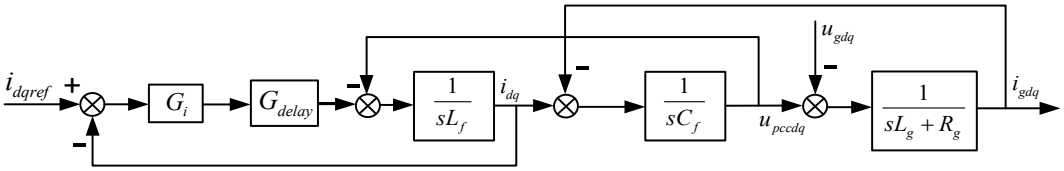

Fig. 5. Control block diagram of the grid-following converter.

III. Stability Analysis Results

To analyze the impact of digital control delay on the stability of grid-following converters, a case study of 7 kW grid-connected converter is built and the key parameters are listed in TABLE I [17].

TABLE I. Parameters of 7 kW Grid-Connected Converter

Grid		
U_g	Grid voltage	220 V
f_g	Grid frequency	50 Hz
L_g	Grid impedance	3.6 mH
R_g	Grid resistance	0.2 Ω
Converter		
U_{dc}	DC-side voltage	700 V
P_{ref}	Rated active power	7 kW
L_f	Filter impedance	2.4 mH
C_f	Filter capacitance	15 μF
f_s	Switching frequency	5 kHz
f_{sa}	Sampling frequency	10 kHz
i_{dref}	d-axis current reference	14.5 A
i_{qref}	q-axis current reference	0 A
ω_{pll}	Bandwidth of phase-locked loop	20 Hz
ω_i	Bandwidth of current loop	350 Hz

Based on the analysis above and the parameters shown in TABLE I. the Nyquist plot of the impedance ratio Y_{inv}*Z_g and Bode plots of the open-loop transfer function G_{open} can be achieved [18].

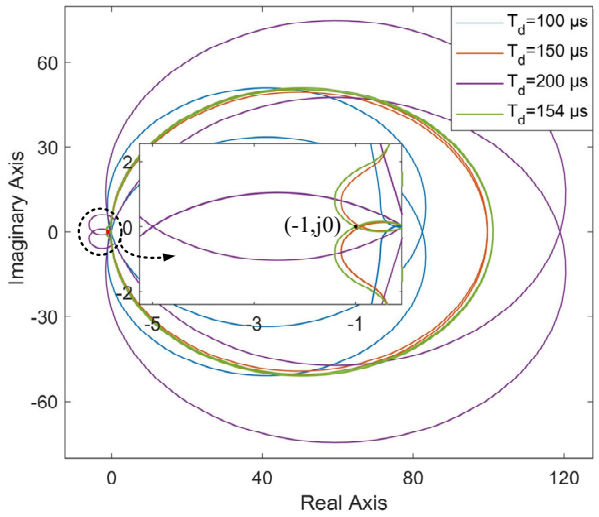

Fig. 6. Nyquist plot of the impedance ratio Y_{inv}*Z_g.

As shown in Fig. 6, when T_d is equal to 100 μs or 150 μs, the Nyquist plot does not encircle the (-1, j0) point, hence, the system is stable. When T_d is equal to 154 μs, the Nyquist plot passes through the (-1, j0) point, which means the system is at a critical stable state. When T_d is larger than 154 μs, the system loses its stability. It is because when the Nyquist plot encircles the (-1, j0) point, it means that the closed-loop system has poles on the right-half of the s-plane.

As shown in Fig. 7, the amplitude-frequency curves with different delay time are the same. When T_d increases, both the gain margin and phase margin decreases. In the presence of negative feedback, the system will become unstable when the phase margin is zero or negative at a frequency where the gain margin exceeds unity. When T_d is equal to154 μs, the gain margin is equal to zero and when T_d is larger than 154 μs, the gain margin becomes negative. Thus, the analysis of the impact of delay on the grid-following converter through the two methods is consistent and the values of T_d for the critical stability are the same.

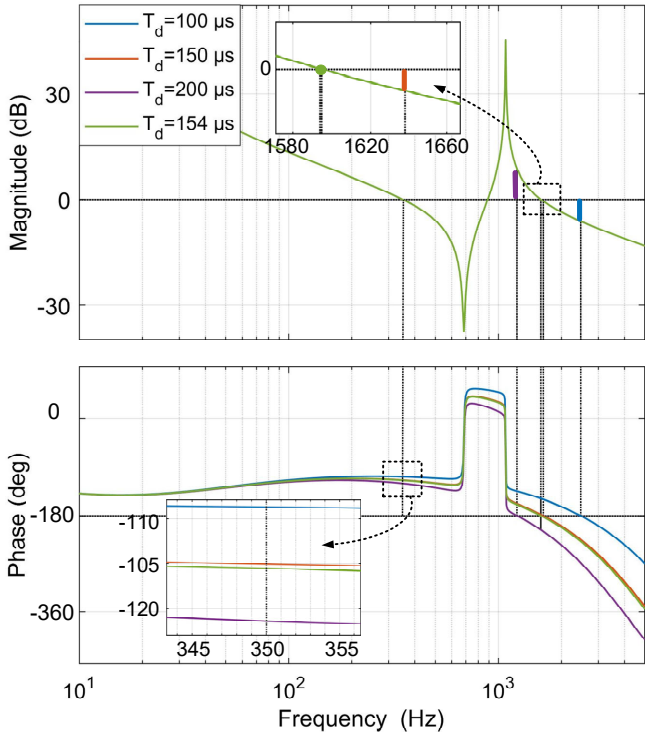

Fig. 7. Bode plots of the open-loop transfer function G_{open}.

IV. Simulation Results

In order to verify the effectiveness of the aforementioned stability analysis, the simulation system is established in

Matlab/Simulink. The parameters are the same as those in Section III.

The simulation results of the PCC voltages and grid currents are shown in Fig. 8. When a unit delay of one sampling period is added at 0.2 s, the voltage and current start oscillate and the system cannot stay stable any more. The simulation result is consistent with the theoretical analysis. When the delay time increases, the system will lose stability.

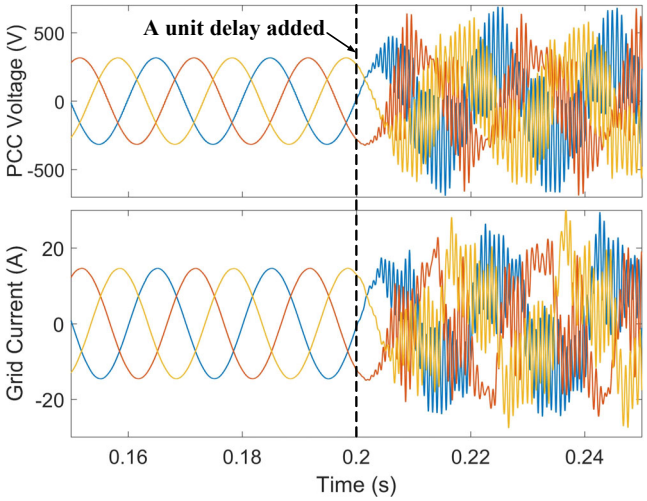

Fig. 8. Simulated waveforms of the PCC voltages and grid currents.

V. Experimental Results

In order to analyze the impact of digital control delay on the stability of grid-following converters, an experimental setup is constructed which is shown in Fig. 9. The grid-connected converter is based on Semikron two-level three-phase voltage source converter and it is controlled by dSPACE MicroLabBox DS1202. The AC power grid is simulated by Cinergia GE & EL20. The DC side is supplied by two Delta Elektronika SM600-10 DC power supply. The experimental parameters are the same as the parameters listed in TABLE I. The experimental waveforms of the PCC voltage and grid current of phase-A are shown in Fig. 10.

As shown in Fig. 10, before the delay unit is added, the system is stable and the current can track the given reference. In this situation, the delay includes one sampling period caused by the computational delay and a half sampling period caused by the PWM delay. When a delay of one sampling period is added, the system starts to oscillate and after a very short oscillation, the converter shuts off. The experimental result is consistent with the theoretical analysis and simulation result.

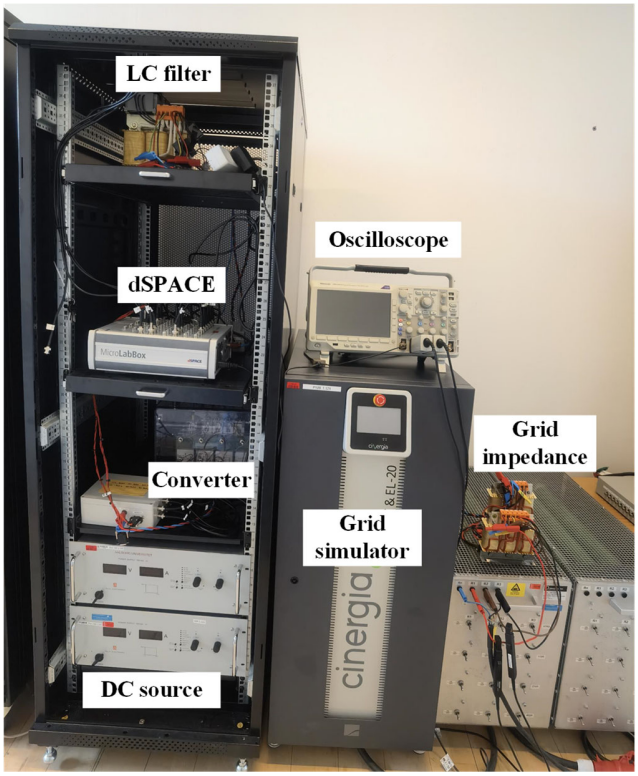

Fig. 9. The experimental setup of a grid-connected system.

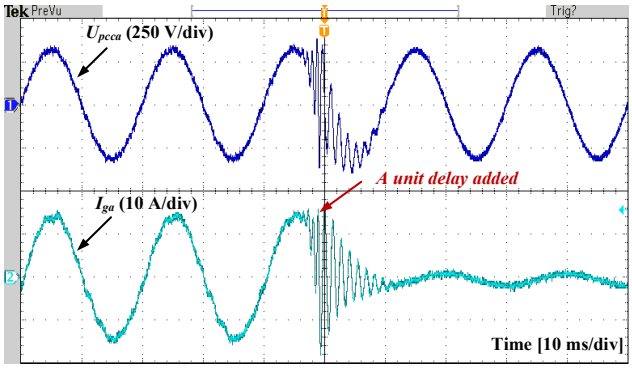

Fig. 10. Experimental waveforms of the PCC voltage and grid current. (CH1: PCC voltage; CH2: grid current)

VI. Conclusion

This paper analyzes the impact of delay on the stability of grid-following converters using the impedance model and the SISO transfer function. When the delay time increases, the system will gradually lose stability. The theoretical analysis results are compared with time-domain simulation results and experimental results. The results of the delay impact on the grid-following converters are consistent.

References

[1] F. Hans, M. Oeltze and W. Schumacher, "A Modified ZOH Model for Representing the Small-Signal PWM Behavior in Digital DC-AC Converter Systems," *IECON 2019 - 45th Annual Conference of the IEEE Industrial Electronics Society*, pp. 1514-1520, 2019.

[2] Y. Tu, J. Liu, Z. Liu, D. Xue and L. Cheng, "Impedance-Based Analysis of Digital Control Delay in Grid-Tied Voltage Source Inverters," *IEEE Transactions on Power Electronics*, vol. 35, no. 11, pp. 11666-11681, Nov. 2020.

[3] Z. Lin, X. Ruan, H. Zhang and L. Wu, "A Generalized Real-Time Computation Method With Dual-Sampling Mode to Eliminate the Computation Delay in Digitally Controlled Inverters," *IEEE Transactions on Power Electronics*, vol. 37, no. 5, pp. 5186-5195, May 2022.

[4] C. Zou, B. Liu, S. Duan and R. Li, "Influence of Delay on System Stability and Delay Optimization of Grid-Connected Inverters With LCL Filter," *IEEE Transactions on Industrial Informatics*, vol. 10, no. 3, pp. 1775-1784, Aug. 2014.

[5] L. Huang, C. Wu, D. Zhou and F. Blaabjerg, "A Simple Impedance Reshaping Method for Stability Enhancement of Grid-Following Inverter Under Weak Grid," *2021 IEEE 12th International Symposium on Power Electronics for Distributed Generation Systems (PEDG)*, pp. 1-6, 2021.

[6] B. Wen, D. Boroyevich, R. Burgos, P. Mattavelli and Z. Shen, "Small-Signal Stability Analysis of Three-Phase AC Systems in the Presence of Constant Power Loads Based on Measured d-q Frame Impedances," *IEEE Transactions on Power Electronics*, vol. 30, no. 10, pp. 5952-5963, Oct. 2015.

[7] J. Sun, "Impedance-Based Stability Criterion for Grid-Connected Inverters," *IEEE Transactions on Power Electronics*, vol. 26, no. 11, pp. 3075-3078, Nov. 2011.

[8] H. Zhang, X. Wang, L. Harnefors, H. Gong, J. Hasler and H. Nee, "SISO Transfer Functions for Stability Analysis of Grid-Connected Voltage-Source Converters," *IEEE Transactions on Industry Applications*, vol. 55, no. 3, pp. 2931-2941, May-June 2019.

[9] C. Guo, S. Yang, W. Liu, C. Zhao and J. Hu, "Small-Signal Stability Enhancement Approach for VSC-HVDC System Under Weak AC Grid Conditions Based on Single-Input Single-Output Transfer Function Model," *IEEE Transactions on Power Delivery*, vol. 36, no. 3, pp. 1313-1323, June 2021.

[10] X. Gao, D. Zhou, A. Anvari-Moghaddam and F. Blaabjerg, "Stability Analysis of Grid-Following and Grid-Forming Converters Based on State-Space Model," *2022 International Power Electronics Conference (IPEC-Himeji 2022- ECCE Asia)*, pp. 422-428, 2022.

[11] D. Yang, X. Ruan and H. Wu, "Impedance Shaping of the Grid-Connected Inverter with LCL Filter to Improve Its Adaptability to the Weak Grid Condition," *IEEE Transactions on Power Electronics,* vol. 29, no. 11, pp. 5795-5805, Nov. 2014.

[12] B. Wen, D. Boroyevich, R. Burgos, P. Mattavelli, and Z. Shen, "Analysis of D-Q Small-Signal Impedance of Grid-Tied Inverters," *IEEE Transactions on Power Electronics*, vol. 31, no. 1, pp. 675-687, Jan. 2016.

[13] X. Wang, L. Harnefors, and F. Blaabjerg, "Unified impedance model of grid-connected voltage-source converters," *IEEE Transactions on Power Electronics*, vol. 33, no. 2, pp. 1775-1787, Feb. 2017.

[14] D. Zhou, and F. Blaabjerg, "Bandwidth oriented proportional-integral controller design for back-to-back power converters in DFIG wind turbine system," *IET Renewable Power Generation*, vol. 11, no. 7, pp. 941-951, 2017.

[15] D. Yang, and X. Wang, "Unified Modular State-Space Modeling of Grid-Connected Voltage-Source Converters," *IEEE Transactions on Power Electronics*, vol. 35, no. 9, pp. 9700-9715, Sept. 2020.

[16] Y. Liao and X. Wang, "Impedance-Based Stability Analysis for Interconnected Converter Systems With Open-Loop RHP Poles," *IEEE Transactions on Power Electronics*, vol. 35, no. 4, pp. 4388-4397, April 2020.

[17] X. Gao, D. Zhou, A. Anvari-Moghaddam and F. Blaabjerg, "Grid-Following and Grid-Forming Control in Power Electronic Based Power Systems: A Comparative Study," *IECON 2021 – 47th Annual Conference of the IEEE Industrial Electronics Society*, pp. 1-6, 2021.

[18] J. Wang, J. D. Yan, L. Jiang and J. Zou, "Delay-Dependent Stability of Single-Loop Controlled Grid-Connected Inverters with LCL Filters," *IEEE Transactions on Power Electronics*, vol. 31, no. 1, pp. 743-757, Jan. 2016.